

Resolution of time–frequency analysis for seismic crosshole measurements

Andrzej Leśniak^{*†}, Hiroaki Niitsuma

Faculty of Engineering, Tohoku University, Sendai 980-77, Japan

Abstract

A sensitive processing method to remove the random components of seismic signals and examine their similarity in the time–frequency domain is presented. We transform signals to the time–frequency (T–F) domain using parametric and nonparametric algorithms. The first method estimates an autoregressive process (AR) and its spectral density in a short moving window, the second computes the instantaneous frequency of the signal at each moment of time. The main problems are the trade-off between the time and the frequency domain which limits the resolution of the method and cross terms of the T–F distribution which may lead to misinterpretation of the different modes of the signal. Next we present some limitation on the resolution of some popular T–F distributions and suggest an improved method based on a time–frequency coherency function. We conclude that coherency analysis in the T–F domain makes it possible to investigate precisely the repeatability of seismic sources, to control the stacking efficiency and also to estimate the onset of the same modes (for example P and S components, tube waves).

1. Introduction

Seismic signals propagated in an inhomogeneous medium possess a complicated structure. Different parts of the recorded signals contain different modes generated by incident waves. The most important modes are body, reflected and refracted waves. In reverse VSP and crosshole measurements tube waves are also generated. These main components of the seismic signals are contaminated by a huge number of scattered and diffracted waves which are excited due to variation of the rock density and elastic coefficients. They compose a coda wave. It is essential to distinguish the particular modes from the coda

in each signal. Unfortunately, some modes which contain important information about the geologic structure (like reflected waves) have relatively low energy compared to, for example, the highly energetic tube waves. Moreover, for high frequency signals time delays between onsets for different modes are small and the frequency range of individual modes and of the coda is similar. This makes standard processing methods difficult to apply.

To distinguish the different modes within the signal we propose to transform it to the T–F domain. This allows us to observe the frequency range of each part of the signal. To distinguish low energy modes in the signal it is necessary to achieve a high resolution T–F distribution. In the second section we examine the resolution of some important classes of the T–F distributions to find which is more suitable for detecting low energy signals.

^{*} Fax: +48-12-331-071; E-mail: lesniak@uci.agh.edu.pl.

[†] On leave from the Institute of Geophysics, University of Mining and Metallurgy, 30-059 Cracow, Poland.

The coherency is low for the coda part of signals which propagate even on closely, adjacent raypaths. The body waves, tube waves and reflected waves recorded on closely spaced sensors remain coherent. In the third section we present a processing method based on the time–frequency coherency function which identifies the coherent components of a tested signal. This method not only helps us to remove spatially incoherent components for each signal but to check the stability of the exciting signal and effectiveness of stacking as well.

2. Time–frequency representation of the seismic signals

Because of their intrinsically complicated structure, seismic signals which propagate in stochastic media can be seldom modeled using stationary, probabilistic models. Since the frequency range of each mode forming the seismic signal may be similar and the particular modes can overlap in time, we have to use a sensitive method of analysis to recover the useful information. Because any time–frequency representation (TFR) estimates the frequency content of the signal at each moment in time, we can use this approach in the analysis of nonstationary signals which change their energy or dominant frequency with time. It is difficult to find a method of evaluation of the TFR that is optimal for all kinds of signals. Generally, we can obtain the TFR of the signal using either nonparametric or parametric methods.

2.1. Nonparametric TFR

A Cohen class consists of the shift invariant nonparametric TFRs (Cohen, 1989). Any TFR from this class is defined as a two-dimensional convolution (marked as $\star\star$) of the Wigner–Ville distribution $W_x(t, f)$:

$$W_x(t, f) = \int_R e^{-i2\pi f\tau} x\left(t + \frac{\tau}{2}\right) x^*\left(t - \frac{\tau}{2}\right) d\tau \quad (1)$$

with a kernel function $\Phi(t, f)$:

$$\text{TFD}_x(t, f; \Phi) = \Phi(t, f) \star\star W_x(t, f) \quad (2)$$

Each kernel $\Phi(t, f)$ represents the particular member

of the Cohen class. Among them the following two are widely used: (1) a Choi–Williams TFR (Choi and Williams, 1989):

$$\Phi(t, f) = \mathcal{F}_\tau^{-1} \left\{ \sqrt{\frac{\sigma}{4\pi}} \frac{1}{|\tau|} \exp \left[-\frac{\sigma}{4} \left(\frac{t}{\tau} \right)^2 \right] \right\} \quad (3)$$

and (2) a spectrogram:

$$\Phi(t, f) = \mathcal{F}_\tau^{-1} \left\{ \gamma \left(-t - \frac{\tau}{2} \right) \gamma^* \left(-t + \frac{\tau}{2} \right) \right\} \quad (4)$$

where \mathcal{F}_τ^{-1} is the inverse Fourier transformation with respect to variable τ and γ is a window of analysis. The spectrogram is identical to that defined using a short time Fourier transform (STFT) as:

$$\text{SPEC}_x^\gamma(t, f) = |\text{STFT}_x^\gamma(t, f)|^2 = \left| \int_k x(k) \gamma^*(k-t) e^{-i2\pi f k} dk \right|^2 \quad (5)$$

2.2. Parametric TFR

The second way of evaluation of the TFR is the parametric method (Kay, 1988). A parametric autoregressive model $\text{AR}(p)$ of the given random signal has a form:

$$x(n) = - \sum_{k=1}^p a_k x(n-k) + \epsilon_k \quad (6)$$

where ϵ is a white noise process with zero mean and variance σ^2 . The power spectrum of $x(t)$ is given by formula:

$$P_x^{\text{AR}}(f) = \frac{\sigma^2}{|1 + \sum_{k=1}^p a_k e^{-i2\pi f k}|^2} \quad (7)$$

The essential requirement for accurate evaluation of the power spectrum in each window is the correct estimation of the coefficients a_k . Various methods has been proposed to obtain the most appropriate set of coefficients (e.g. Yule–Walker, Burg, minimum variance and others).

If we define the analysis window $w(n_0 - n, l)$ as:

$$w(n_0 - n, l) = \begin{cases} 1 & \text{for } n_0 - l \leq n \leq n_0 \\ 0 & \text{for others} \end{cases} \quad (8)$$

the short time window of $x(n)$ at time n_0 is defined

as $x_{n_0}(n) = x(n)w(n_0 - n, l)$. The AR(p) model of time frequency distribution is defined as $P_{x_i}^{AR}(t, f)$.

2.3. Resolution of the TFRs

In order to test the effectiveness of the T–F representations in detecting low energy components we have modeled three crossing chirp signals (signals with a linear modulation of the frequency and a Gaussian envelope):

$$s_k(t) = \Omega_k e^{-A_k(t-t_k)^2 + i2\pi C_k(t-t_k)^2 + i2\pi B_k(t-t_k)} + n(t) \quad k = 1, 2, 3 \quad (9)$$

where $n(t)$ represents white noise. They are pre-

sented on Fig. 1. Frequency ranges for the first and second chirps are from 200 Hz up to 1250 Hz and for the third from 200 Hz up to 800 Hz. The maximum amplitude of the last chirp is 10 times smaller than the two others. The signal to noise ratio was set at 16 dB for the two first components and 6 dB for the third, small energy chirp. Our aim was to identify this last signal.

To obtain the nonparametric TFR of the signal $s(t) = s_1(t) + s_2(t) + s_3(t)$, we have used the Welch algorithm (Welch, 1967) to evaluate the windowed spectrogram and Choi–Williams method as a representation from the Cohen class. As regards the parametric method, we adopted the Burg method using the Akaike Information Criterion (AIC) (Akaike,

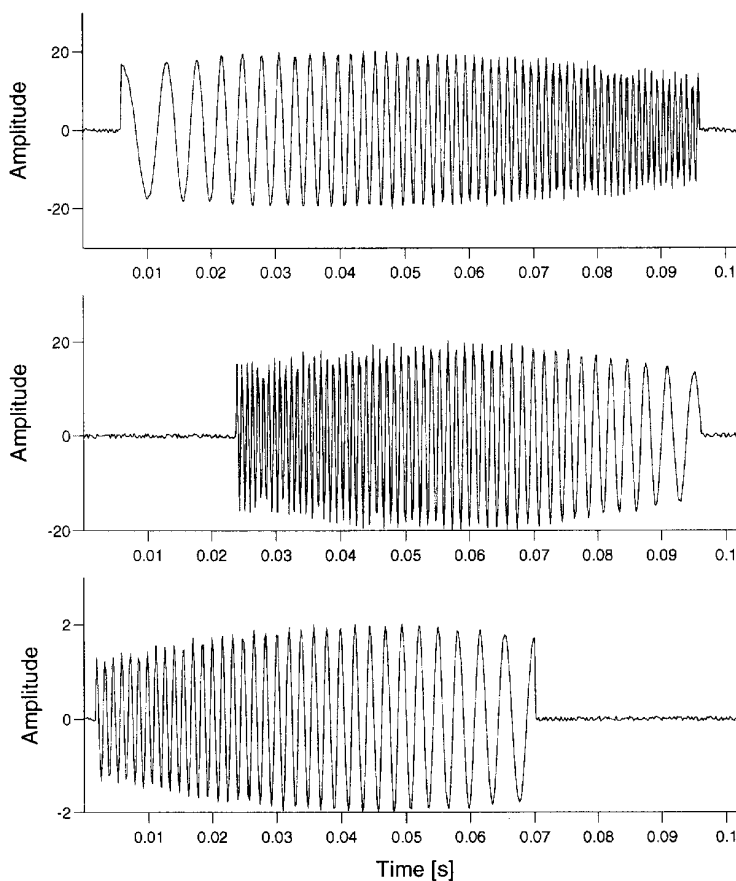


Fig. 1. Three synthetic chirp signals used in analysis. (a) Chirp signal with increasing, instantaneous frequency, (b) chirp signal with decreasing, instantaneous frequency, (c) chirp signal with decreasing, instantaneous frequency with maximum amplitude ten times lower than the first and the second chirp signals.

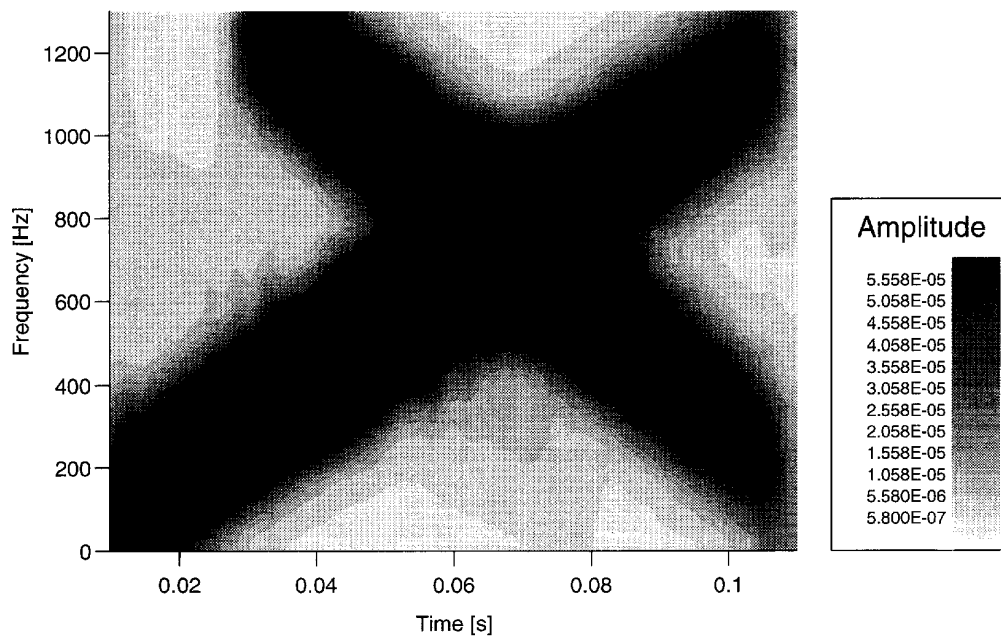


Fig. 2. Spectrogram of the sum of three chirp signals.

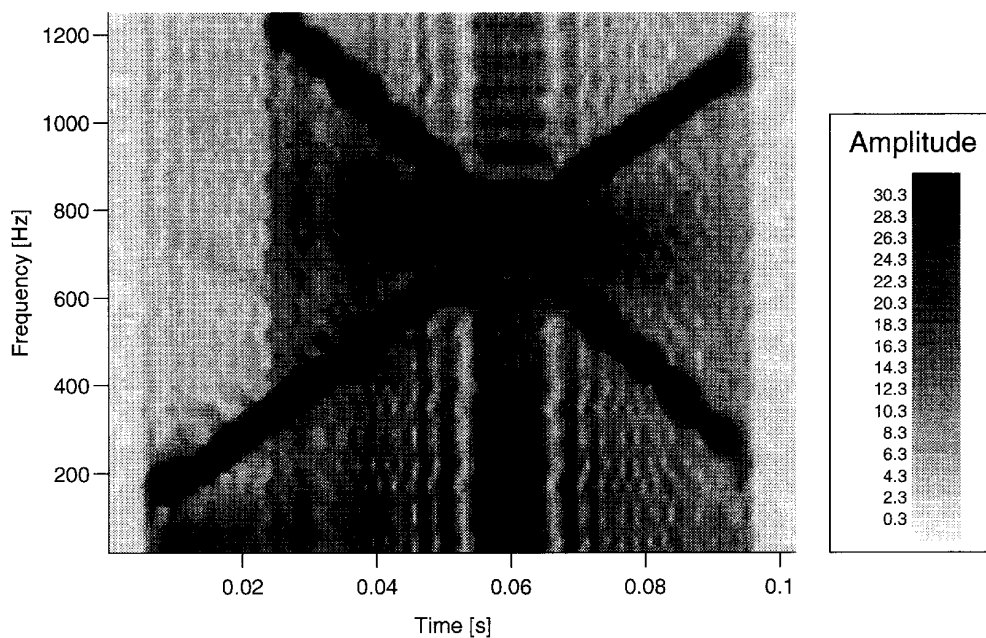


Fig. 3. Choi-Willians time-frequency representation of the sum of three chirp signals.

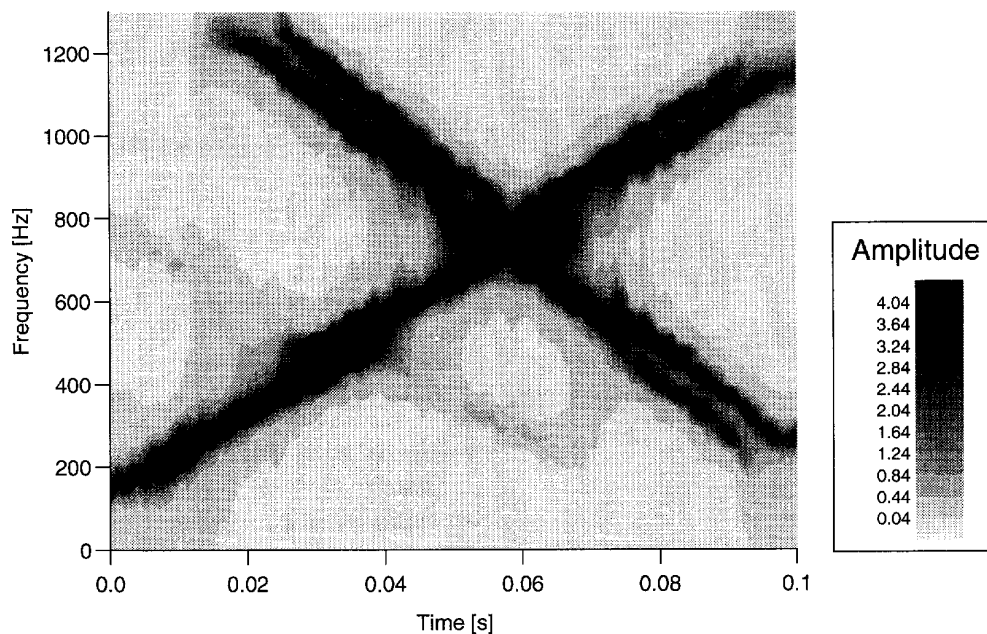


Fig. 4. Autoregressive time–frequency representation of the sum of three chirp signals.

1984) to determine the order of the AR process in each window separately. Because the signal (9) is not autoregressive the AIC tends to select maximum order allowed by interpretator. The length of the analysis window was set to the maximum wavelength of modeled signal. The variation of the chirp signal frequencies inside the window of analysis is equal to 117 Hz, 145 Hz and 120 Hz for first, second and third chirp signals, respectively.

The following figures present the results of the analysis. The shading scale on each figure varies from 10% to 0.1% of the maximum amplitude. The resolution of the spectrogram in Fig. 2 is limited because of trade-off between the time and frequency domain. For any time the estimated frequency range inside the analysis window is twice or even greater than the theoretical one. The Choi–Williams representation (Fig. 3) properly estimates the frequency contents in each window but the cross terms destroy the resolution. The cross terms always exist in this representation, especially if two signals overlap in time or in frequency (which is common for many seismic signals). The third signal has too small an energy to be detected by either of these methods. It

was only possible to detect it using the AR modelling (Fig. 4) but this result suffers because of the high variance of the TFR and the splitting of the maximum peak of the spectrum.

In conclusion we can say that it is difficult to improve the detectability of small energy signals by increasing sophistication of the algorithms for the evaluation of the TFRs alone. The results will be worse compared with present examples if the noise is not white and if the S/N ratio is lower.

3. Time–frequency coherency of the seismic signals

Let us assume that we are interested only in the coherent waves recorded by two sensors located relatively close to each other. In practice, components of the recorded waveform such as body waves and tube waves are only time delayed and preserve their similarity if we compare them on the adjacent sensors. If the velocity inhomogeneities in the rocks are smaller than the dominant wavelength, they excite coda waves with an isotropic energy distribution

(Sato, 1984). Even if the sensors are located close to each other, the recorded coda possesses a low coherency contrary to the body, reflected and tube waves (Leśniak et al., 1995). One method used to detect the coherent components in time varying signals is a generalization of the stationary cross spectral analysis methods.

3.1. Time–frequency coherency function

A quantity called the time–frequency coherency (TFC) was defined by White and Boashash (1990) to determine the similarity of the nonstationary signals:

$$\hat{C}_{xy}(t, f) = \frac{\hat{S}_{xy}(t, f)}{\sqrt{\hat{S}_x(t, f)\hat{S}_y(t, f)}} \quad (10)$$

where \hat{S} is an estimator of the time–frequency spectrum or cross spectrum. It was shown that TFC has useful properties for cross spectral analysis. It can be interpreted as a time and frequency dependent correlation coefficient. Values near zero over a wide frequency range indicate that the processes are nearly

uncorrelated at that time, while values near unity suggest that processes are linearly dependent.

It is important to characterize the class of admissible estimators of the time–frequency coherency function. We can use either parametric or nonparametric methods for evaluating the short time power spectrum. It is essential to note that for nonparametric estimators the particular TFR must be positive for all signals and thus the parametrization of the kernel $\Phi(t, f)$ cannot directly depend on signal. As may be seen from the previous subsection, the Choi–Williams representation is not positive for all signals. Even the class of positive T–F distributions defined by Cohen and Posch (1985) is not admissible for estimation of the TFC function because the kernel of the positive TFR with correct marginals is dependent on the signal. As regards nonparametric estimators, it was shown that only smoothed spectrograms are properly defined (White and Boashash, 1990).

Because of the poor resolution of the spectrogram in both time and frequency domains we can also use the parametric autoregressive model of the power spectrum. The estimator $P_x^{\text{AR}}(t, f)$ of the time–

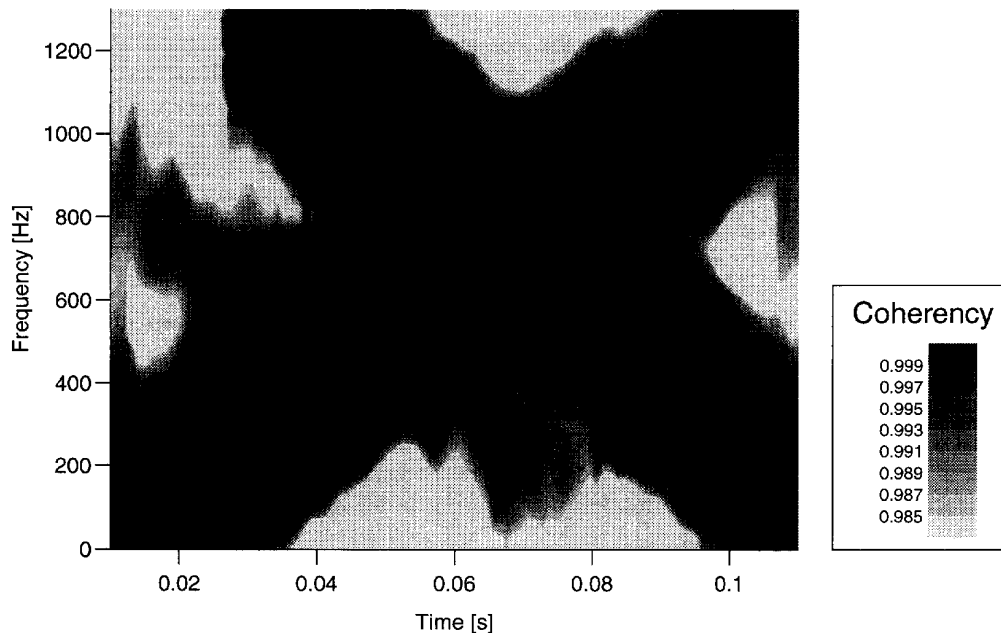


Fig. 5. Time–frequency coherency of the three chirp signals — spectrogram method.

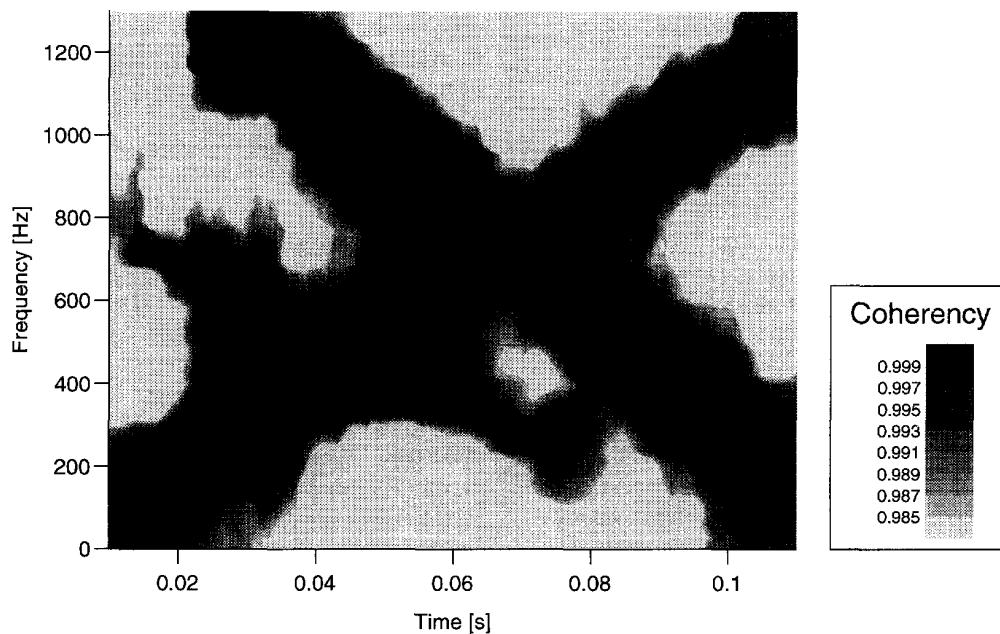


Fig. 6. Time–frequency coherency of the three chirp signals — autoregressive modelling.

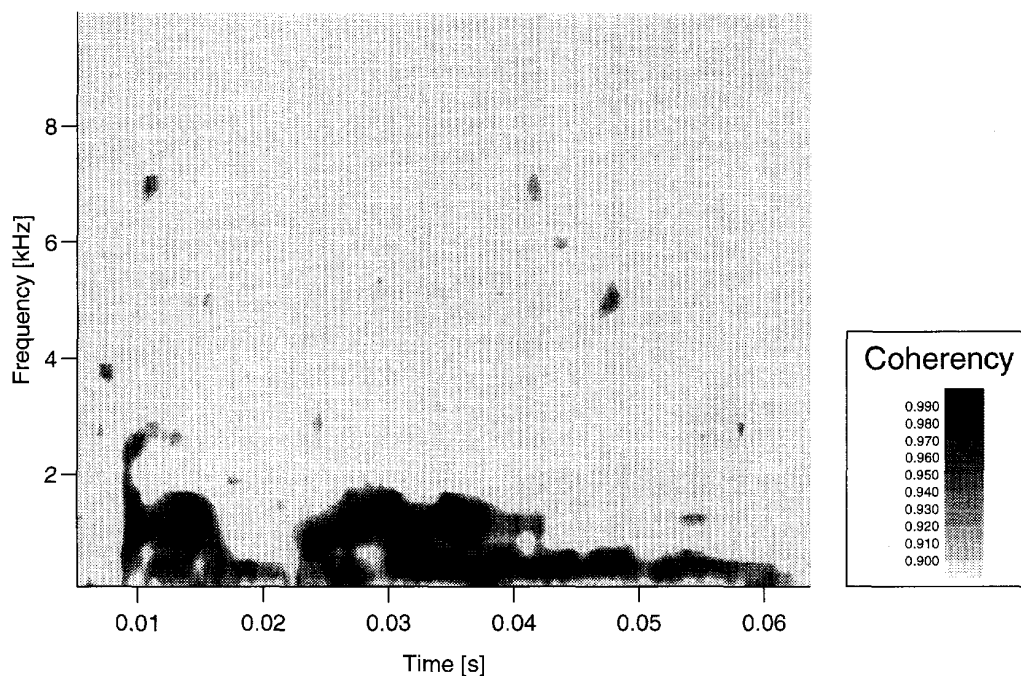


Fig. 7. Time–frequency coherency between signals recorded at the same position of the detector before stacking.

frequency spectrum \hat{S} is always positive and, as it will be shown, possesses good resolution.

3.2. Resolution of the *T–F* coherency function

To test this method for detecting small, coherent signals we have evaluated the TFC function between two signals consisting of the same 3 chirp signals from Fig. 1 with white noise sequences added to each signal. A mean value of the coherency between the white noise signals is equal 0.6. We have applied the spectrogram (Fig. 5) and the AR power spectrum (Fig. 6) as estimators of the time–frequency spectrum or cross spectrum. Contrary to the TFR method (Fig. 5) both the TFC functions identify the low energy chirp. The function based on the spectrogram enlarges the frequency range inside the window, especially for higher energy chirps in the same way as the TFR function. The frequency resolution for the second function is better than for the first one, but the variance of this estimator is higher. In spite of the small amplitude of the third chirp (almost

equal to the amplitude of the noise) it was possible to evaluate correctly its time and frequency content using both methods.

3.3. Application of the time–frequency coherency to the seismic signals

We have shown using the TFC function, that we can detect in both time and in frequency relatively small, similar signals buried in low coherency noise. This makes it possible to apply the TFC method to the examination of the similarity of seismic signals. We have used crosshole seismic signals excited by an air-gun and measured by a 3C seismic detector (Niitsuma, 1989) in a Higashi–Hachimantai field, Japan. The distance between the detector located in well EE-4 at depth 360 m and the air-gun located in the E-3 well at depth 372 m was about 25 m. The geologic structure at the depth, where the detector was set, consists of homogeneous tuff with a thin silt layer at a depth of 385.4 m in the E-3 well acting as a strong reflector. Our first aim was to examine the

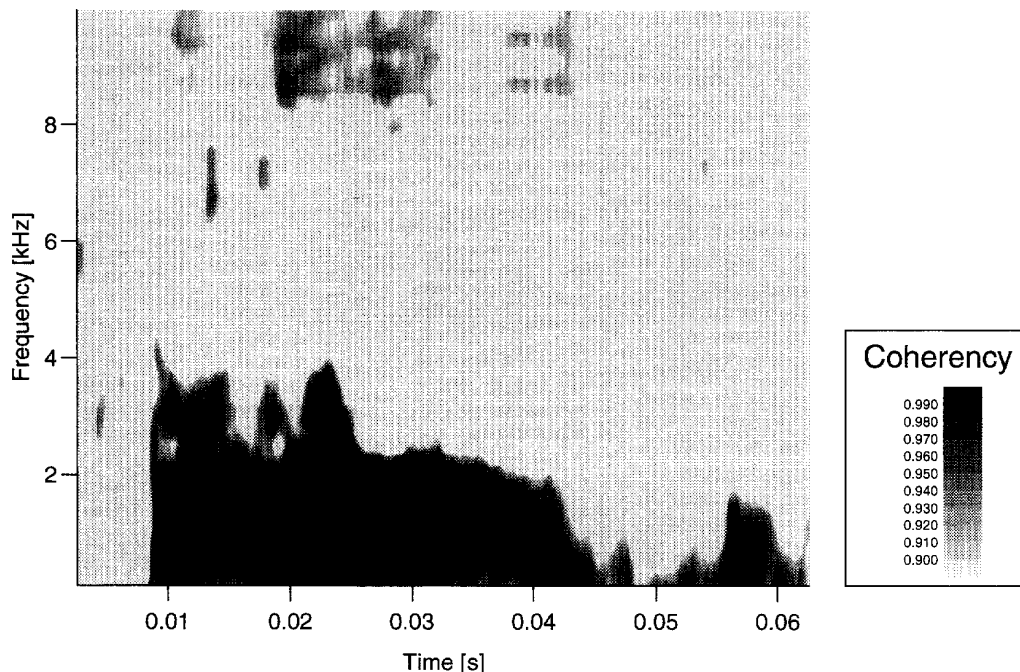


Fig. 8. Time–frequency coherency for two stacked signals.

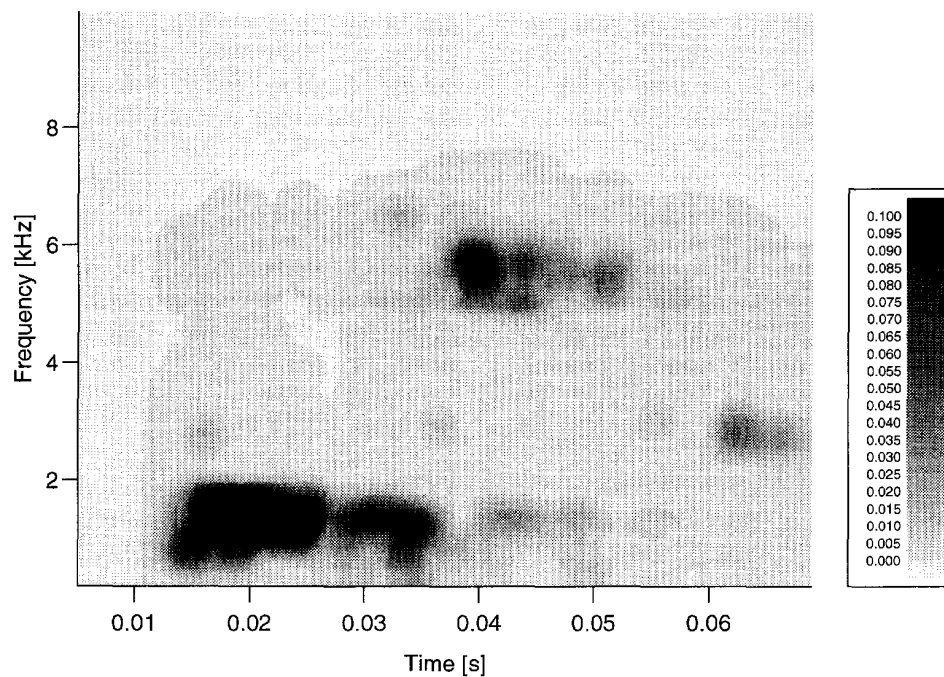


Fig. 9. Time–frequency representation of stacked signals recorded at depth 372 m.

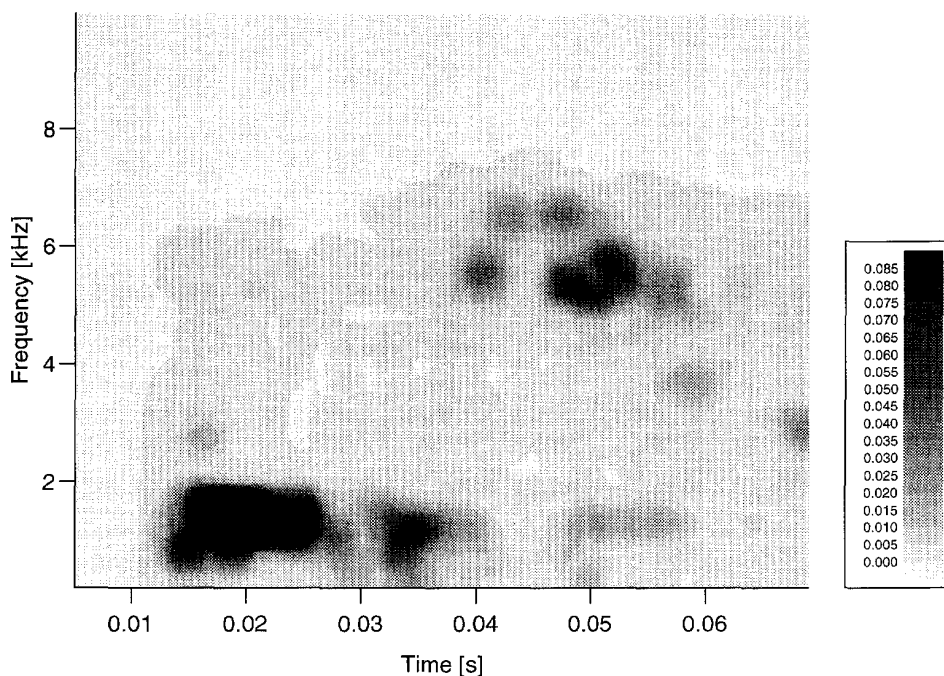


Fig. 10. Time–frequency representation of stacked signals recorded at depth 374 m.

repeatability of the air-gun source by computing the TFC between the signals excited at the same position before stacking. The result is presented in Fig. 7. Two waveforms are coherent over a wide frequency range (up to 4 kHz) at the beginning of the record and then the high coherency region gradually decreases to lower frequencies. The coherent parts of the signals can be used as a source of information for further interpretation.

To reduce the incoherent components of the signals and increase the repeatability of the method we have twice stacked 10 different signals recorded at the same position of the air-gun to create two stacked signals. To examine the efficiency of stacking for increasing the similarity we have compared these two stacked signals using the T–F coherency function. The result for the X component is shown on Fig. 8. The stacked signals are again coherent up to 4

kHz at the beginning of the record, then coherency falls to 2 kHz and below. Comparing with Fig. 7 a significant enhancement of the signal similarity after stacking, especially in high frequency range, can be seen.

To identify the different modes of the signals recorded in the crosshole experiment we have evaluated the TFR and TFC for two adjacent positions of the sensor. In Fig. 9 and Fig. 10 the two T–F distributions of the signal recorded by the X-component of the sonde located at depths of 372 m and 374 m are presented. In each position of the air-gun 10 shots were stacked. It is impossible to distinguish any mode except the P wave. In Fig. 11 the TFC between these signals is given. The signals are mainly coherent in the low frequency range. It is important to note that only small parts of the adjacent signals are coherent. The isolated areas with high coherency

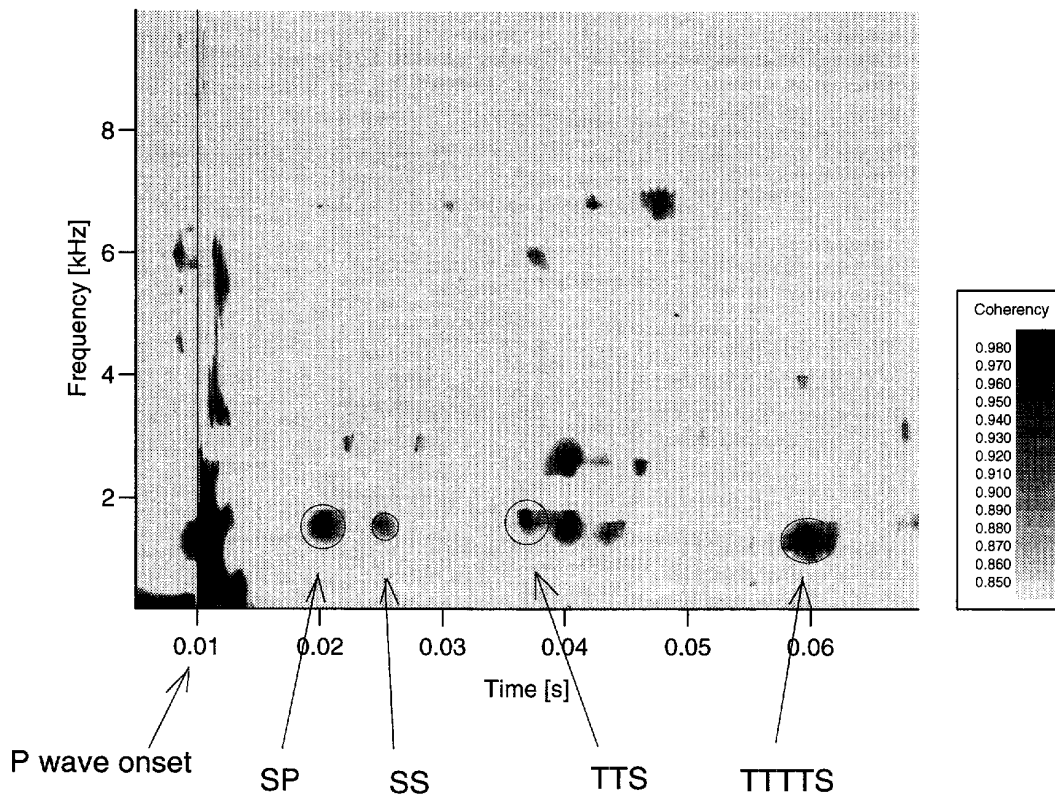


Fig. 11. Time–frequency coherency between the stacked signals recorded at depths of 372 m and 374 m.

(over 0.85) are supposed to be the onset of the coherent, direct, reflected or secondary waves generated by the air-gun. Because the geology and velocity structure of this area is known, it is theoretically possible to evaluate the onset of some important modes which are expected to be recorded. In Fig. 11 converted shear wave (SP), reflected wave (SS) and secondary P and S waves generated by the tube wave (TTS,TTTS) have been identified.

4. Conclusion

In this paper we have investigated the utility of TFR and TFC for detecting low energy coherent components in seismic signals. Using the TFR method it was only possible to localize the small energy chirps using AR modeling of the power spectrum. The resolution of the spectrogram was insufficient and the Choi–Williams method was too insensitive to recover the low energy signal. Remarkable improvement was achieved by using the TFC function. The estimators based not only on AR modeling but also on the spectrogram were able to localize low energy signals. Using this method we can precisely investigate the repeatability of the signals excited by an air-gun, control the stacking and remove incoherent, scattered components from the signals.

References

- Akaike, H., 1984. A new look on statistical model identification. *IEEE Trans. Automatic Control*, AC-19: 716–723.
- Choi, H.I. and Williams, W.J., 1989. Improved time–frequency representation of multi-component signals using exponential kernels. *IEEE Trans. Acoust., Speech Sig. Proc.*, ASSP-37(6): 862–871.
- Cohen, L., 1989. Time–frequency distribution — A review. *Proc. IEEE*, 77(7): 941–981.
- Cohen, L. and Posch, T.E., 1985. Positive time–frequency distribution functions. *IEEE Trans. Acoust., Speech Sig. Proc.*, Vol. ASSP-33(1): 31–37.
- Kay, S., 1988. Spectral estimation. In: J.S. Lin and A.V. Oppenheim (Editors), *Advanced Topics in Signal Processing*. Prentice Hall, Englewood Cliffs, NJ, pp. 58–122.
- Leśniak, A., Moriya, H. and Niitsuma, H., 1995. Time–frequency coherency analysis for crosshole seismic measurements. *Proc. 3rd SEGJ/SEG International Symposium on Geotomography and Fracture Imaging*, Tokyo, Japan, pp. 94–101.
- Niitsuma, H., 1989. Downhole AE measurement technique and its application to geothermal fields. *J. Acous. Emis.*, 7(4): 201–209.
- Sato, H., 1984. Attenuation and the envelope formation of three-component seismograms of small local earthquakes in randomly inhomogeneous lithosphere. *J. Geophys. Res.*, 89(B2): 1221–1241.
- Welch, P.D., 1967. The use of fast Fourier transform for the estimation of power spectra: a method based on time averaging over short modified periodograms. *IEEE Trans. Audio-Electroacoust.*, AU-15(6): 70–73.
- White, L.B. and Boashash, B., 1990. Cross spectral analysis of nonstationary processes. *IEEE Trans. Information Theory*, 36(4): 830–835.